Bhoo-Kampan Vol. 1, pp. 21-45, December 2014

http://bhookampan.co.in/index
Journal of Indian Society of Earthquake Science
ISSN: 2320-6217

Moho Depth Variation in Shillong-Mikir Hills Plateau and its Adjoining Region of Northeastern India Estimated from Reflected and Converted Waves

Dipok K. Bora[1*], Saurabh Baruah[2] and Rajib Biswas[3]

[1.] Department of Physics, Diphu Government College, Diphu, Karbi Anglong-782 462, Assam, India.
[2.] Geoscience Division, CSIR North-East Institute of Science and Technology, Jorhat-785 006, Assam, India.
[3.] Department of Physics, Tezpur University, Tezpur-784 028, Assam, India.

Abstract

In this study an attempt is made to estimate the depth distribution of Mohorovičić (Moho) discontinuity beneath the Shillong-Mikir plateau and its adjoining region of northeast India. We have used 195 earthquakes that are recorded by the permanent broadband network during 2001-2009 in this region. The first P and S wave arrivals, reflected P (PmP) and S (SmS), converted P to S (PS) and S to P (SP) waves at the Moho discontinuity are precisely identified and analyzed. A total of 956 reflected (PmP and SmS) phase arrival times of 172 shallow (depth $\leq$25 km) earthquakes and 70 converted (PS and SP) phases from 23 intermediate depth (with depth > 38 km) earthquakes are used. The results show that the Moho depth beneath the Shillong plateau is 33.5 - 37.0 km, and it is deeper, about 39.0 - 41.0 km beneath the Brahmaputra valley to the north.

Key words: Reflected waves, converted waves, Moho discontinuity, Shillong plateau, Northeast India.

1. Introduction

The Shillong-Mikir plateau (SMP) in the Northeast Region (NER) of India, latitude (25^0 to 27.5^0 N) and longitude (90^0 to 94^0 E), is seismically very active region where 3 large (M ≥ 7.0) earthquakes (Kayal, 2008) and the 1897 great M_S=8.7 earthquake occurred (Oldham, 1899). The 1897 great Shillong earthquake caused extensive destruction in the region killing about 1,540 lives with a property loss of $30 million (Tillottson, 1953) at that time. The region lies in the seismic zone V of India (BMTPC 2003). The zone V is the maximum rating zone in the national seismic zoning map of India. The SMP is a part of the Indian

*** Corresponding author: E-mail Address:**
dipok23@gmail.com **(Dipok K. Bora)**

shield, which is separated out from the peninsular shield, and moved to the east by about 300 km along the Dauki fault (Evans, 1964). The E-W trending Dauki fault separates the plateau to the north and the Bengal basin to the south (Kayal, 2001) (Fig 1). The River Brahmaputra, on the other hand, separates the plateau from the Himalaya to the north. The E-W segment of the river at the northern boundary of the plateau is named Brahmaputra fault (Nandy, 2001). The Mikir massif, a part of the Shillong plateau, moved to the northeast along the ~300 km long NW-SE trending Kopili fault (Baruah et al. 1997; Nandy, 2001).

Several hundred earthquakes (M > 4.0) are recorded during the past few decades in the region. In addition to the national network run by the India Meteorological Department (IMD), the North-East Institute of Science and Technology-Jorhat (NEIST-J), the National Geophysical Research Institute, Hyderabad (NGRI-H) and several universities established analog networks since 1982. These stations are now upgraded to broadband digital stations with global positioning system (GPS) timing since 2001.

Several studies (Sitaram et al. 1986; De and Kayal 1990; Rai et al. 1999; Sitaram et al. 2001; Kayal and Zhao 1998; Bhattacharya et al. 2005, 2008, 2010) have been carried out to estimate the Moho depth of northeastern (NE) India in general and that of the SMP in particular using the analog data recorded before 2001. With the recent broadband waveform data accrued from these stations allowed few researchers to adopt receiver function analysis (Kumar et al. 2004; Mitra et al. 2005; Ramesh et al. 2005) to estimate the depth of Moho. Recently Bora and Baruah (2012) studied the variation of Moho depth by using the reflected seismic waves. They inferred a gently dipping Moho reaching a depth of 41 km to the north of Shillong plateau. Based on gravity model, constrained by broadband seismological data, Nayak et al. (2008) suggested that the Moho beneath the Shillong plateau exists at a shallow depth of about 35 km.

No study is, however made to estimate the Moho depth using both the reflected and converted phases of the local earthquakes recorded by broadband network in the region. Precise reading of reflected phases in the analog records of earlier seismic network was difficult. With the advent of digital seismic network, precise detection of reflected and converted phases, made it possible to estimate crustal discontinuities (Horiuchi et al. 1982a, b and Nakajima et al. 2002). In this study, we have utilized reflected (PmP and SmS) and converted (PS and SP) phases from seismic waveforms of the local earthquakes to estimate the depth of the Moho discontinuity in the SMP region.

2 Tectonic Setting

The northeastern region of India comprises distinct geological units, like the Himalayan frontal arc to the north, the highly folded Indo-Burma mountain ranges to the east, the Brahmaputra alluvium in the Assam valley and the Shillong-Mikir plateau between these two arcs, and thick sediments of the Bengal basin to the south of the Shillong plateau (Fig

1). Seismotectonics of the region has been the subject of several studies (e.g., Tapponier et al. 1982; Kayal and De 1991; Kayal 1996, 2001; Kayal et al. 2006, Angelier and Baruah 2009, Nandy 2001, Baruah et al. 2010). Bilham and England (2001), based on geodetic and GPS data, proposed a 'pop-up' tectonic model of the Shillong plateau, and argued that the great June, 12, 1897 (Oldham, 1899) earthquake was produced by a south dipping hidden fault at the northern boundary of the Shillong plateau; they named it the 'Oldham fault' that extends from a depth of about 9 km down to 45 km. They further suggested that the Shillong plateau earthquakes are caused by the 'pop-up' tectonics between the Dauki fault and the Oldham fault. The northwest-southeast trending long Kopili fault separates the Shillong plateau from its fragment part, Mikir Hills. The Assam valley is an east-northeast-west-southwest trending narrow valley, which lies between Shillong plateau and the eastern Himalayan tectonic domains. Details of seismicity and tectonics of the region are reviewed by Kayal et al. 2006; Rajendran et al. 2004; Kayal 2008; Baruah and Hazarika 2008, Baruah et al. 2010, Bora and Baruah, 2012. The prominent geological units of the northeast India region remain geophysically less studied owing to the inaccessibility of this terrain.

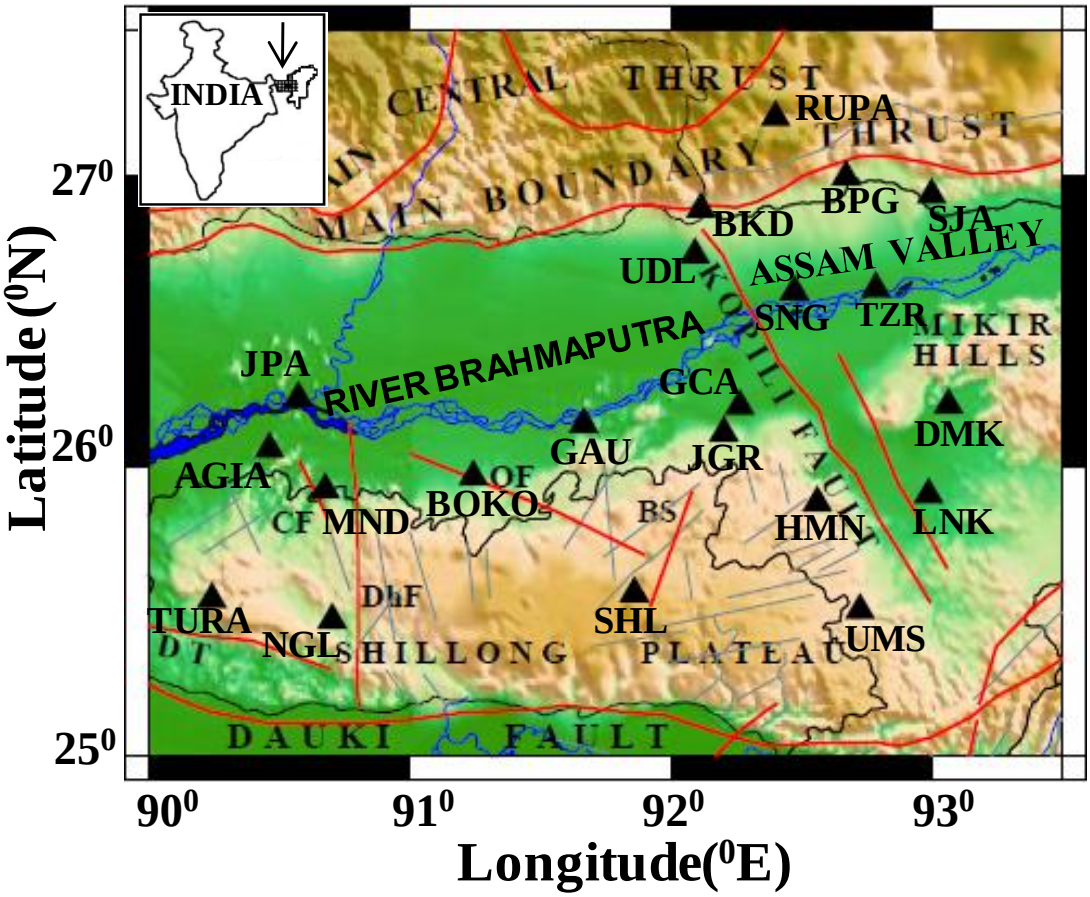

Figure 1. Map showing the major tectonic features of the study region. The digital broadband seismic stations are shown by black triangles. The major tectonic features in the region are indicated: Main Central Thrust, Main Boundary Thrust, Kopili Fault, Dauki Fault, Dh F: Dudhnoi Fault; DT: Dapsi Thrust; OF: Oldham

Fault; CF: Chedrang Fault; BS: Borapani Shear Zone. The light grey lines indicate the minor lineaments. *Inset* Map of India indicating the study region (arrow mark).

3 Data Analysis

3.1 Data

In this study, we utilized 195 earthquakes recorded during 2001-2009 by the local seismic network (NEIST-J and NGRI-H). Locations of the seismic stations with major tectonic features of the study region are shown in Fig.1. The selected events are recorded with higher signal-to-noise ratio and having clear direct, reflected and converted phases. In addition to the NEIST-J and NGRI-H network data, the data of the India Meteorological

Table 1 Station names along with abbreviations

No	Station	Abbreviations	Latitude (^{0}N)	Longitude (^{0}E)	Elevation (meters)
1	Jogighopa	JPA	26.239	90.575	42
2	Manikganj	MND	25.924	90.676	40
3	Nangalbibra	NGL	25.472	90.702	330
4	Gauhati University	GAU	26.152	91.667	69
5	Shillong	SHL	25.566	91.859	1590
6	Bhairabkunda	BKD	26.890	92.115	210
7	Rupa	RUPA	27.203	92.401	1470
8	Seijusa	SJA	26.938	92.999	150
9	Tezpur	TZR	26.617	92.783	140
10	Dokmok	DMK	26.216	93.062	200
11	Bhalukpung	BPG	26.999	92.671	130
12	Golchepa	GCA	26.214	92.265	56
13	Hamren	HMN	25.880	92.560	520
14	Jagiroad	JGR	26.119	92.203	64
15	Lanka	LNK	25.905	92.985	90
16	Singri	SNG	26.608	92.474	60
17	Udalguri	UDL	26.732	92.094	97
18	Umrangso	UMS	25.507	92.726	641
19	Boko	BOKO	25.969	91.244	50
20	Agia	AGIA	26.066	90.464	75
21	Tura	TURA	25.546	90.243	305

Department (IMD), Indian Institute of Geomagnetism (IIG), Gauhati University, Manipur University and Mizoram University are also incorporated for better determination of hypocentral parameters. All these stations are operated both in continuous mode and trigger mode, and data are recorded at a rate of 100 samples per second. The recorded seismograms have been corrected by using an instrument response based on the eloctrodynamic constant, critical damping, natural frequency of seismometers and bit weight of unit gain of each recording unit at all stations. Table 1 shows the digital stations with the abbreviations used. Epicenters of the selected earthquakes located within the latitude 25^0 N to 27.5^0 N and longitude 90^0 E to 93.5^0 E are shown in Fig. 2

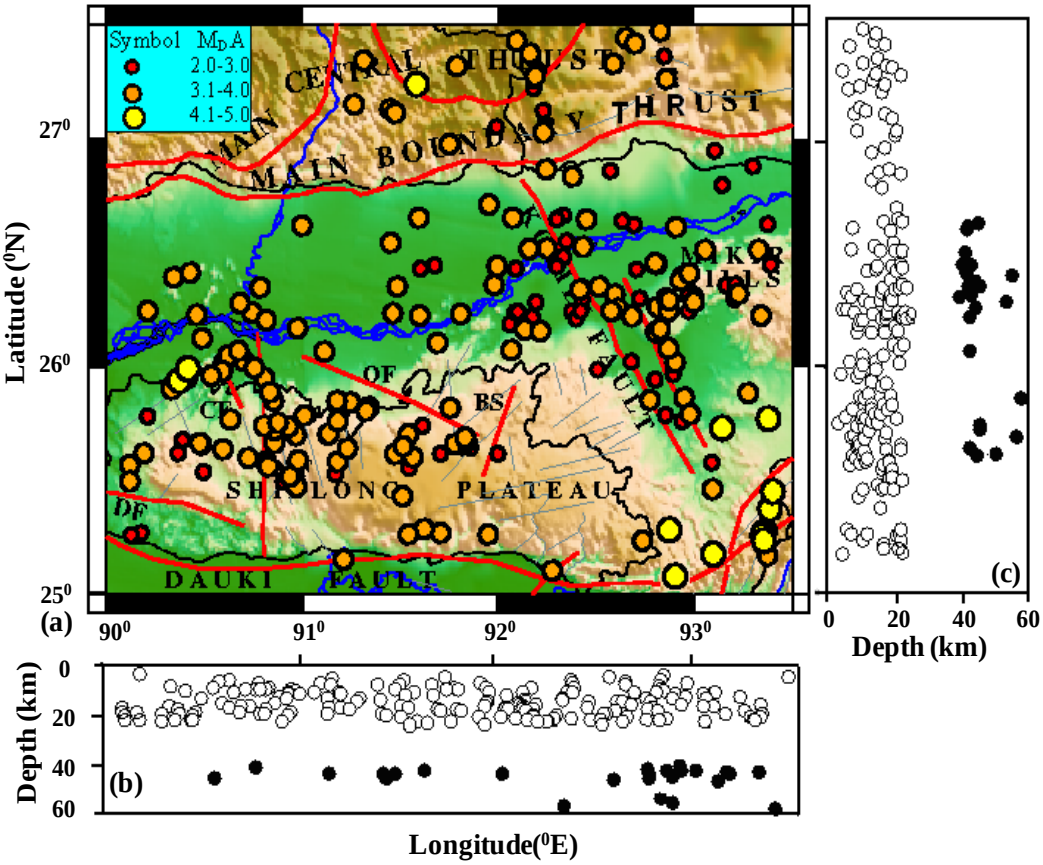

Figure 2. Hypocentral distributions of earthquakes along with depth sections. a Open and solid circles denote shallow and intermediate-depth earthquakes, respectively illustrated by different magnitude range. b Depth section plot along Longitude. c Depth section plot along Latitude.

Precision of hypocenter determination depends not only on the distribution of the recording stations but also on velocity structure between source and stations, particularly in an area where lateral heterogeneities are extreme (Okada et al. 1970). The epicenters are determined using the HYPOCENTER location program of Lienert et al. (1986) based on the crustal velocity model of Bhattacharya et al. (2005) and Baruah et al. (2010).

Uncertainties involved in the estimates of epicenters show that 85 percent of the events are located with 0-2 km error in depths. Simultaneously uncertainties involved in epicenter and error in origin times are of the order of 0-0.5 s., respectively. Duration magnitude (M_D) of the events is estimated in the range 1.7-5.2. Out of 195 selected earthquakes, 172 are located with focal depth ≤ 25 km and 23 earthquakes with focal depth > 38 km (below the Moho depth) in the studied region. The epicentral distance ranges from 70 km to 200 km. We read travel time differences PmP-P and /or SmS-S for the shallower (depth $\leq$ 25 km) events, and PS-P and S-SP from for the deeper (depth > 38 km) events. Altogether 480 reflected P (PmP) and 476 reflected S (SmS) arrivals from the seismograms of 172 crustal earthquakes are identified following the criteria established by Nakajima et al. (2002).

3.2 Reflections from the Moho discontinuity

Prominent phases after the first P- and S- wave arrivals are well identified in seismograms of shallow earthquakes. These phases are interpreted as reflected P (PmP) and S (SmS) waves at the Moho. An example of three component seismograms and particle motion of P, PmP, S and SmS phases are illustrated in Fig.3. When critically examined, the amplitudes of the PmP and SmS phase are found to be larger than that of the first P and S phases. These reflected phases are confirmed by their particle motions. An analytical illustration of particle motions of the reflections is exemplified in Fig.3b. The S and SmS phases are examined using both the transverse and radial components. Although we can pick S phase from any of the two horizontal components, we picked the S and SmS from the same component to avoid any time delay. The accuracy in reading travel time differences of PmP-P and SmS-S is estimated to be 0.1-0.2 s. Fig 3c shows a schematic illustration of the ray paths.

3.3 Converted phases in Moho discontinuity

Some 70 converted (SP and PS) seismic phases of 23 intermediate depth earthquakes are utilized following the criteria established by Matsuzawa et al. (1986, 1990), and Nakajima et al. (2002). These converted SP phases from Moho discontinuity are observed 2.5 to 5.5 s before the first S-phase arrival, and the PS phases 2.4 to 5.2 s after the first P-phase arrival. An example of rotated three component seismograms and particle motion of P, SP, PS and S phases are illustrated in Fig 4 and Fig.5.

4 Estimation of Moho depth

The objective of this work is to estimate the depth of Moho by using travel times data of the direct (P and S), reflected (PmP and SmS) and converted (PS and SP) waves. We

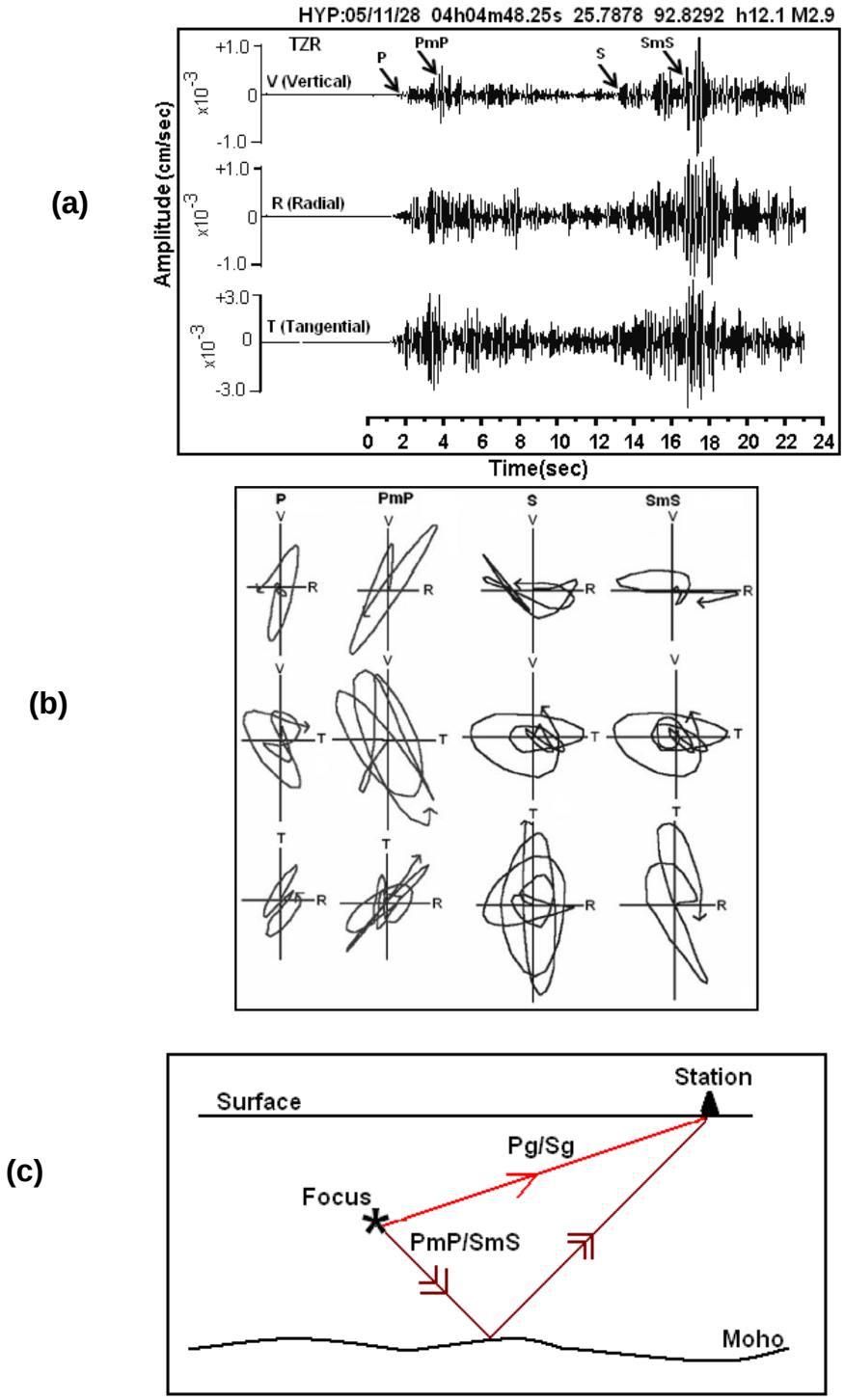

Figure 3. **(a) An example of rotated three-component seismogram of a shallow earthquake recorded at station TEZPUR (TZR). Prominent later phases (PmP and SmS) can be seen after the first P- and S-wave arrivals, respectively. (b) Particle motions of P, PmP, S and SmS phases are also shown. Hypocentral parameters of the event are indicated. (c) A schematic illustration of ray paths of direct (Pg/Sg) and Moho-reflected (PmP/SmS) waves used in this study. Focus of the earthquake event is denoted as ✶ while (▲) indicate a recording station at surface**

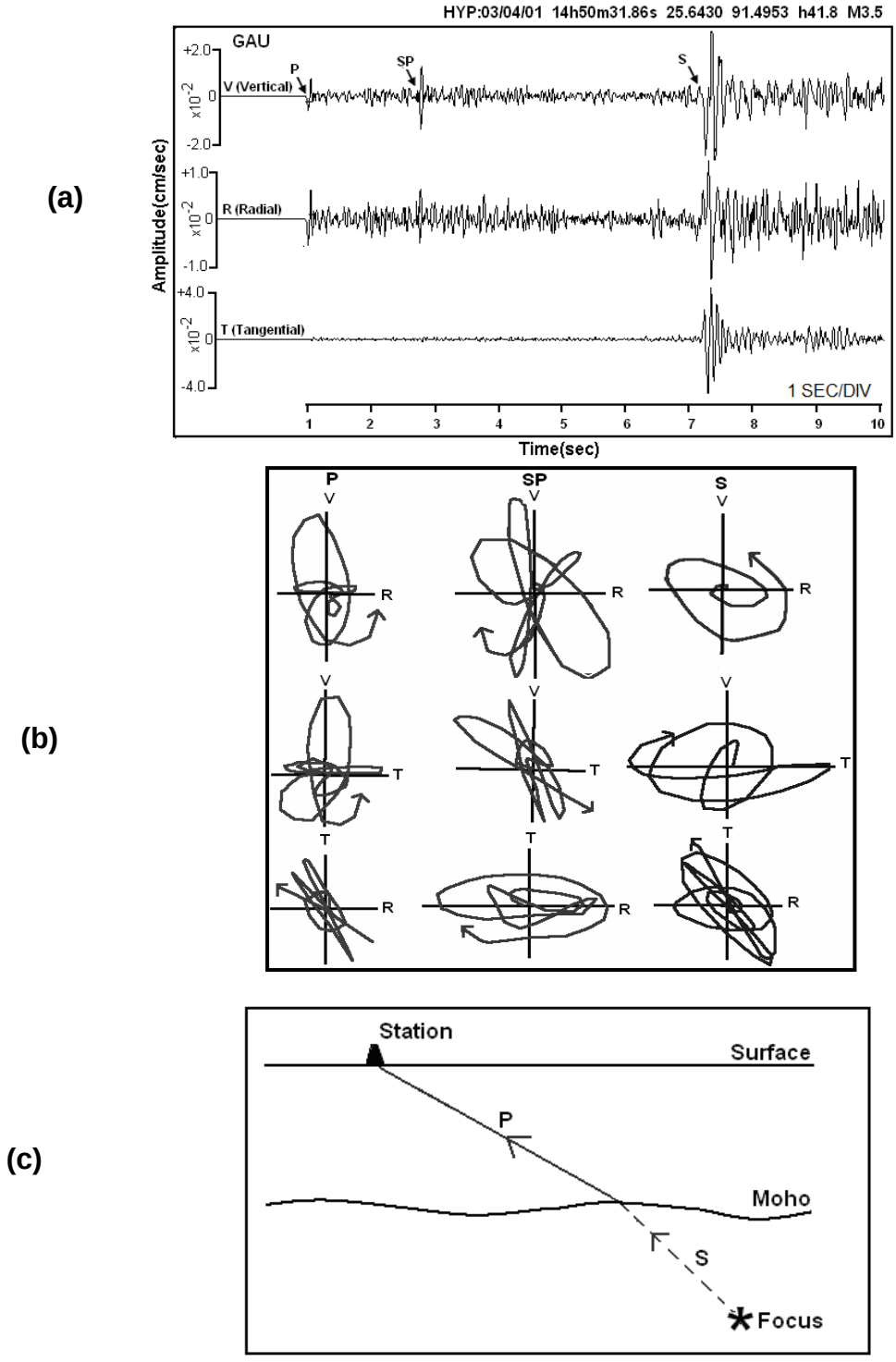

Figure 4. (a) An example of rotated three-component seismogram of an intermediate depth earthquake recorded at a station GAUHATI (GAU). A prominent later phase (SP) can be seen about 4.3 s before the S-wave arrival. (b) Particle motions of P, SP and S phases are also shown. Hypocentral parameters of the event are indicated. (c) A schematic illustration of a ray path of S-to-P converted wave at the Moho. * indicates the focus of the earthquake event, while (▲) indicate a recording station at surface.

follow the method of Nakajima et al. (2002) which is modified form of Horiuchi et al. (1982a, b), Matsuzawa et al. (1986, 1990) and Zhao et al. (1990, 1992).

The Moho depth distribution (*Hm*) is expressed as a function of latitude and longitude in the form of power series as follows:

$$H_m(\phi', \lambda') = C_0 + C_1\phi' + C_2\lambda' + C_3\phi'^2 + C_4\phi'\lambda' + ... + C_{14}\lambda'^4 \qquad (1)$$

where $\phi' = \phi - 26.2, \lambda' = \lambda - 92.1$, ϕ and λ (in degree) are the differences in latitude and longitude between any point and the center of the stations. C_K is the unknown parameters and are determined by the inversion of the observed travel time data. If the Moho boundary is sufficiently gentle, its shape can be expressed by only lower order terms of eq. (1).

4.1 Inversion

The difference between observed and theoretical travel times, $T^{Obs}_{P_2-P_1} - T^{Cal}_{P_2-P_1}$ is expressed as

$$T^{Obs}_{P_2-P_1} - T^{Cal}_{P_2-P_1} = (\frac{\partial T_{P_2}}{\partial \phi_E} - \frac{\partial T_{P_1}}{\partial \phi_E})\Delta\phi_E + (\frac{\partial T_{P_2}}{\partial \lambda_E} - \frac{\partial T_{P_1}}{\partial \lambda_E})\Delta\lambda_E + (\frac{\partial T_{P_2}}{\partial H_E} - \frac{\partial T_{P_1}}{\partial H_E})\Delta H_E + \sum_K (\frac{\partial T_{P_2}}{\partial C_K} - \frac{\partial T_{P_1}}{\partial C_K})\Delta C_K + e \qquad (2)$$

where

$T^{obs}_{P_2-P_1}$ =the observed P_2-P_1 time (i.e. P_2=PmP, SP or PS and P_1=P)

$T^{Cal}_{P_2-P_1}$ =the calculated P_2-P_1 time (i.e. P_2=PmP, SP or PS and P_1=P)

ϕ_E, λ_E and H_E= source parameter (lat, long and depth)

$\Delta\phi_E$, $\Delta\lambda_E$ and ΔH_E = corrections of source parameters

ΔC_K = correction factor of unknown parameters

e= error.

Since the coefficients of $\Delta\phi_E$, $\Delta\lambda_E$ and ΔH_E in eq. (2) is very small, this parameter may be neglected. Then eq. (2) becomes

$$T^{Obs}_{P_2-P} - T^{Cal}_{P_2-P_1} = \sum_K (\frac{\partial T_{P_2}}{\partial C_K} - \frac{\partial T_{P_1}}{\partial C_K})\Delta C_K + e \qquad (3)$$

Here, the partial derivatives of T are

$$\frac{\partial T}{\partial C_K} = \frac{\partial T}{\partial H_m}\frac{\partial H_m}{\partial C_K} = \frac{\partial T}{\partial H_m}\phi'\lambda' \qquad (4)$$

Partial derivative of *Hm* against C_K can be easily calculated from equation (1).

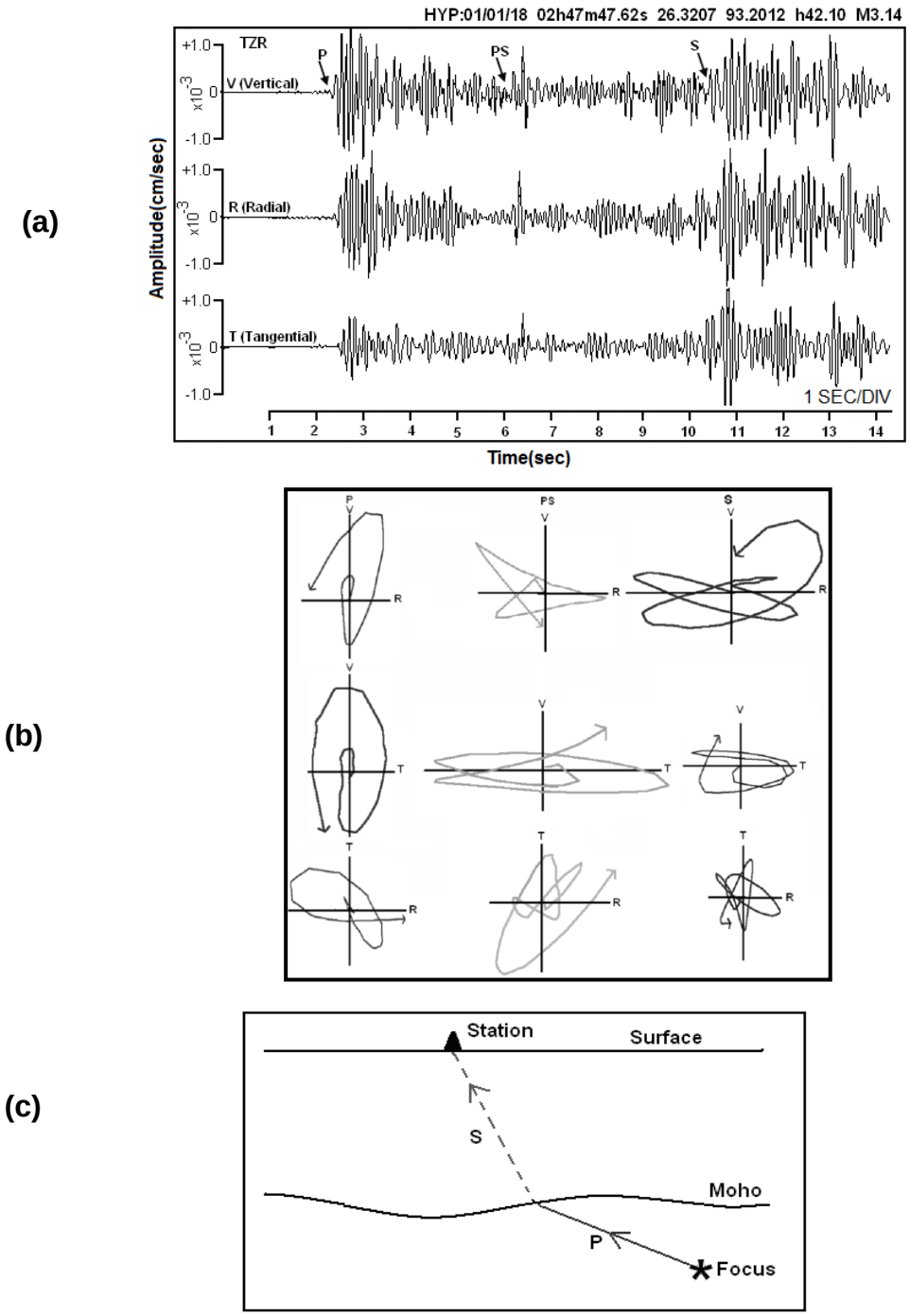

Figure 5. a. An example of rotated three-component seismogram of an intermediate depth earthquake recorded at station TEZPUR (TZR). A prominent later phase (PS) can be seen about 3.5 s after the P-wave arrival. b. Particle motions of P, PS and S phases are also shown. Hypocentral parameters of the event are indicated. c. A schematic illustration of a ray path of P-to-S converted wave at the Moho. * indicates the focus of the earthquake event, while (▲) indicate a recording station at surface.

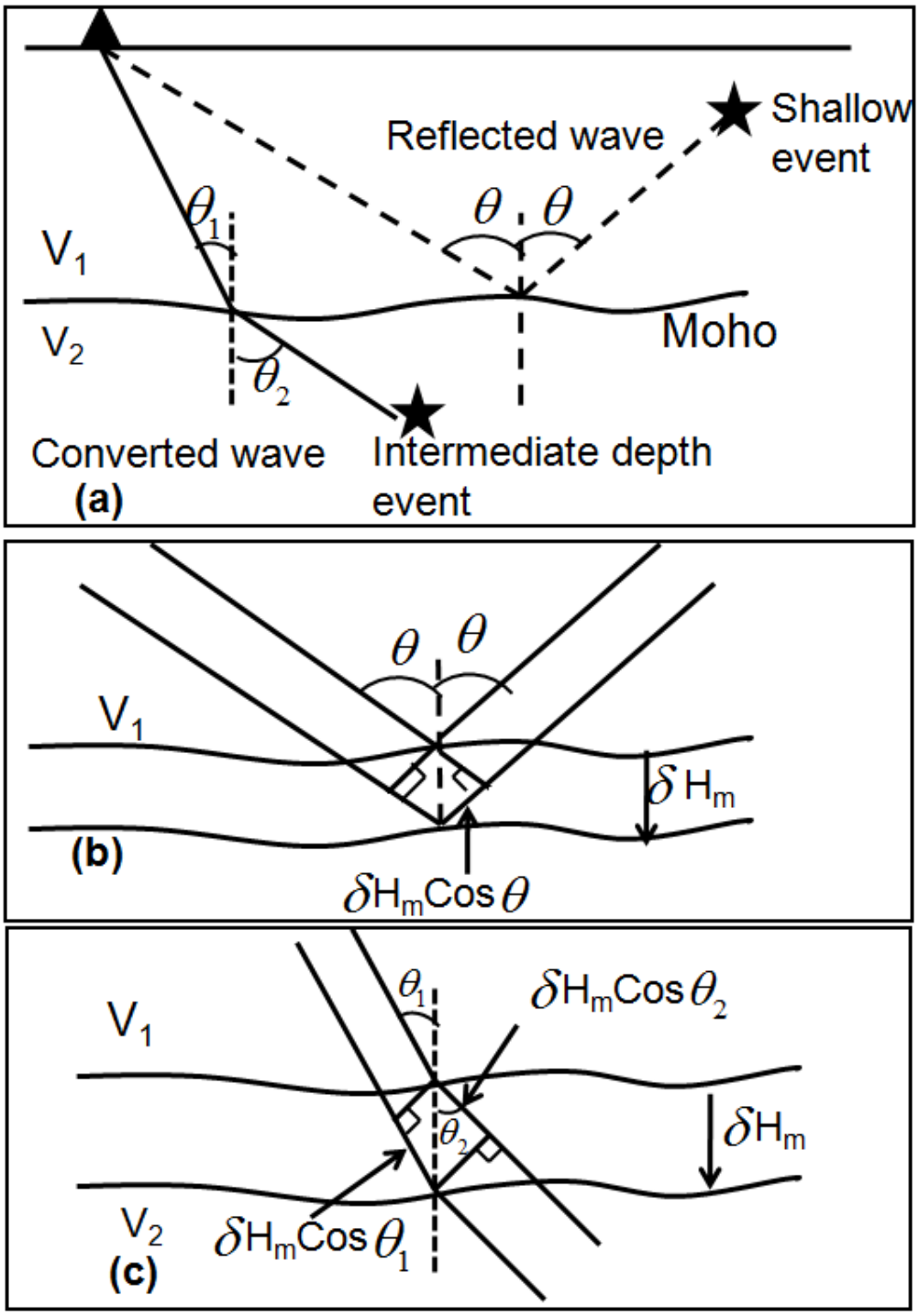

Figure 6. (a) A schematic illustration of ray paths of reflected and converted waves at the Moho.V_1 and V_2 denote the velocity in each medium. θ shows incident angle of reflected waves. θ_1 and θ_2 represent emergent and incident angles of converted waves, respectively. (b) Travel time change of reflected waves due to the depth change of the Moho. (c) Travel time changes of converted waves due to the depth change of the Moho.

4.2 Reflected Phase

Two cases of ray paths at the Moho are considered: (i) the ray propagates in medium 1 (V_1) and is reflected at the interface with medium 2 (V_2) and (ii) the ray propagates from the medium 2 to the medium 1 (Fig. 6a). When the interface is moved in downward direction by δHm, the length of ray path in medium 1 increases by 2δHmCosθ for the reflected wave, where θ is the incident angle of the reflected wave (Fig. 6b).

The travel time change for the reflected wave due to depth change of the interface is expressed by

$$\partial T = \frac{2\partial H_m Cos\theta}{V_1}$$

and the same can be obtained as

$$\frac{\partial T}{\partial H_m} = \frac{2Cos\theta}{V_1} \qquad (5)$$

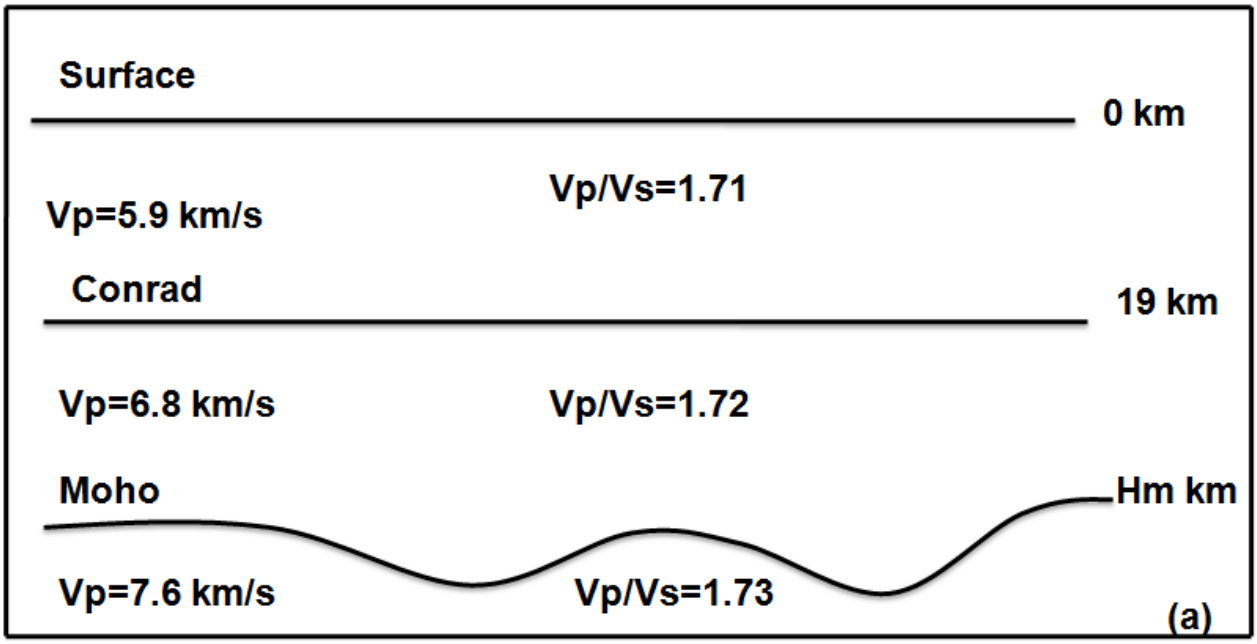

Figure 7. The velocity structure used for the travel time calculation.

4.3 Converted Phase

Similarly, in case of conversion, if the conversion interface is moved by δHm to deeper range, the length of ray path in medium 1 increases by $\delta HmCos\theta_1$ and the travel time increases by $\delta HmCos\theta_1/V_1$. . The ray path in the medium 2, on the other hand, decreases by $\delta HmCos\theta_2$ allowing travel time also to decrease by $\delta HmCos\theta_2/V_2$ (Fig. 6 c), where θ_1 and θ_2 are the emergent and incident angles of converted wave measured from the vertical axis, respectively.

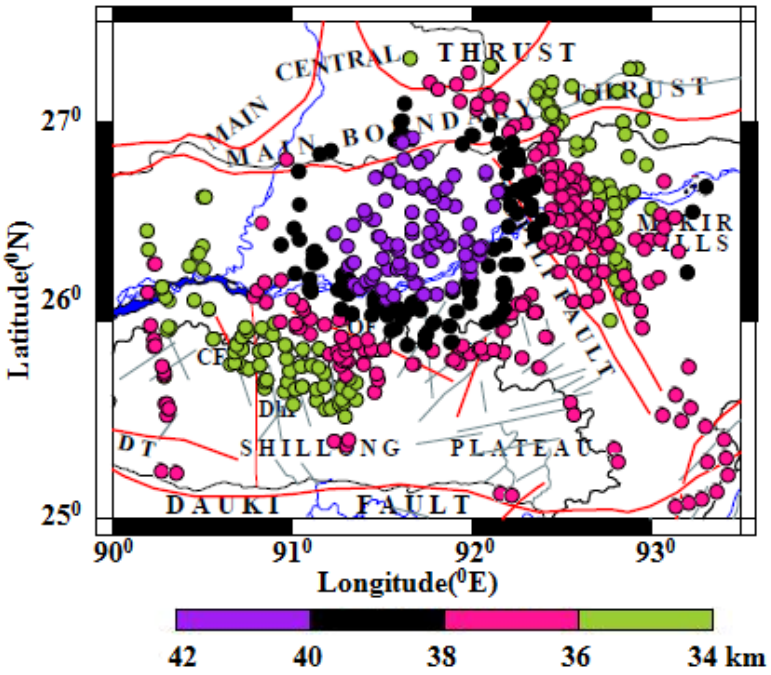

Figure 8. Moho depth obtained for each reflection points. Color scale at each point shows the Moho depth by assuming the flat Moho.

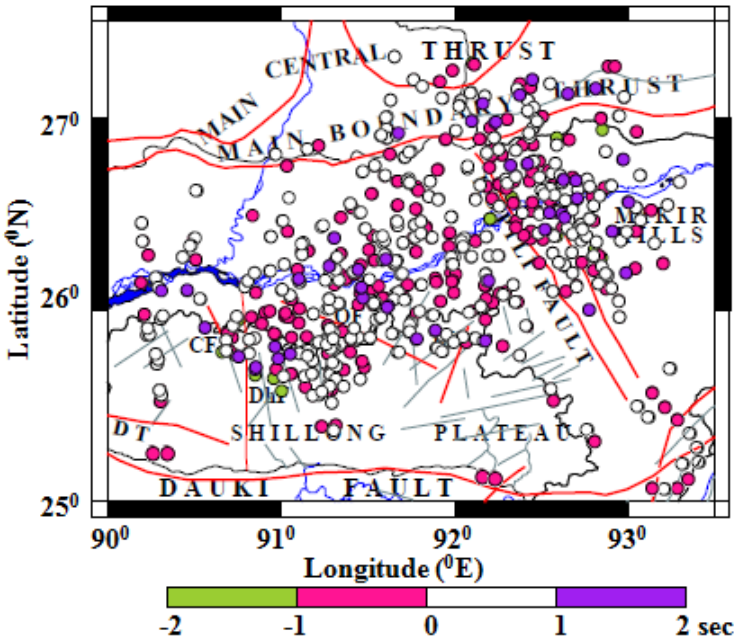

Figure 9. Distribution of reflection points of PmP and SmS waves at Moho. The color scale at each point shows travel time residual between observed and theoretical travel time differences.

Therefore the total travel time change due to the change in depth of the conversion interface can be expressed by

$$\partial T = \partial T_1 - \partial T_2$$
$$= \frac{\partial H_m Cos\theta_1}{V_1} - \frac{\partial H_m Cos\theta_2}{V_2}$$

and can be deduced as

$$\frac{\partial T}{\partial H_m} = \frac{Cos\theta_1}{V_1} - \frac{Cos\theta_2}{V_2}$$

Correlating the simplest approach to the inverse problem, the difference between observed and theoretical travel time as in eq. (3) can be expressed by matrix form as

d=Gm+e (6)

where d= column vectors of residuals between observed and theoretical travel time differences.

G= a matrix of partial derivatives.

m= a column vector of correction term of unknown parameters.

e= an error vector.

The eq. (6) can be written in matrix notation as

G^Td=G^TG m (6a)

which is a normal equation and G^TG is a square matrix, implies to be an inverse. Further G^TG is symmetric, which means that its eigen values are real and non-negative. Therefore, an equation of the form below can be solved with the least squares method

m= $(G^TG)^{-1}G^T$d (6b)

A correction term ΔC_K is added to C_K and $C_K+\Delta C_K$ is used in place of C_K. This calculation is carried out iteratively until ΔC_K becomes sufficiently small. The iteration assumes a flat Moho geometry in initial model.

The variance (square of standard deviation) i.e. σ^2 of *Hm* is expressed as

$$(\partial H_m)^2 = \sigma^2 \sum_i \sum_j D_{ij} C_i C_j H_i(\phi', \lambda') H_j(\phi', \lambda') \quad (7)$$

where D_{ij} is the covariance between the i^{th} (C_i) and j^{th} (C_j) co-efficient in eq. (1) and

$$\sigma^2 = \frac{\sum (T^{Obs} - T^{Cal})^2}{N - 15} \quad (8)$$

where N and 15 are the number of observations and unknown parameters, respectively. (e.g. Horiuchi et al. 1982a, b; Ohmi and Hori 2000).

4.4 Velocity Model

The under study area is divided into three layers which correspond to the upper crust, lower crust and uppermost mantle, respectively. The P and S wave velocities in each layer are assumed to be constant. We assigned P- wave velocity to be 5.9 km/s in the upper crust, 6.8 km/s in the lower crust and 7.6 km/s in the uppermost mantle. The S wave velocity is obtained by assuming Vp/Vs to be 1.71 in the upper crust, 1.72 in the lower

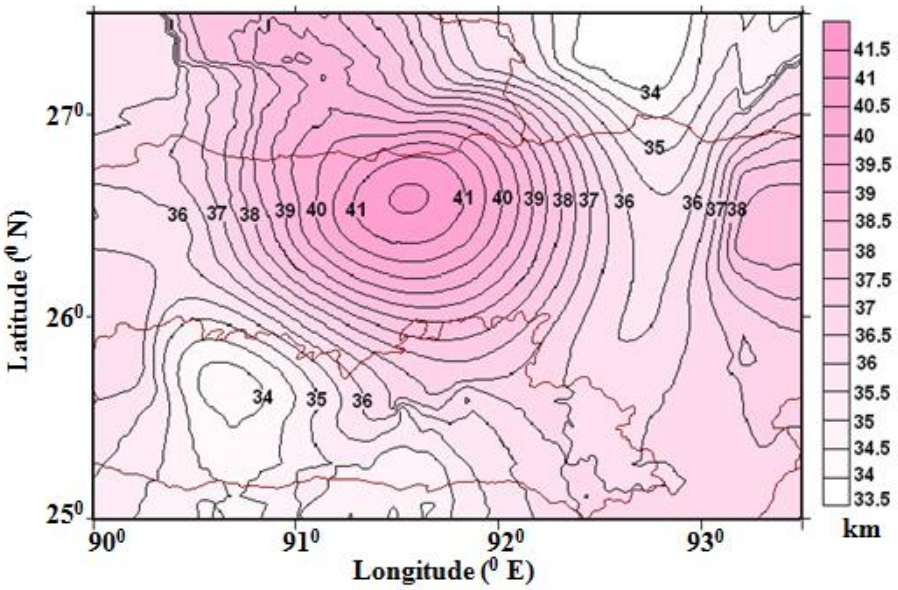

Figure 10. **Depth distribution of Moho obtained at the reflection points. Depth to the Moho is shown by contours with 0.5 km interval. The corresponding color scale is shown along with.**

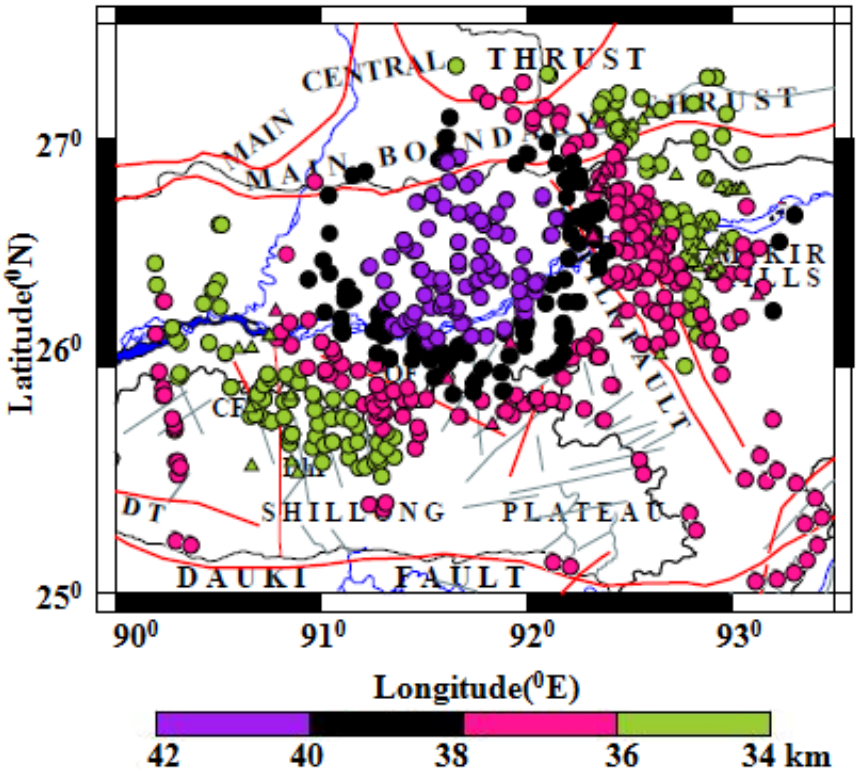

Figure 11. **Moho depth obtained for each data point. Circles and triangles denote reflection and conversion points, respectively. Color scale at each point shows the Moho depth by assuming the flat Moho**

Table 2 Inverted values of unknown parameters for the Moho depth using reflected phases.

Coefficients	Values
C_0	38.612953
C_1	-5.200471
C_2	3.586749
C_3	-2.917659
C_4	-5.296921
C_5	-1.769319
C_6	4.888841
C_7	-1.636553
C_8	2.631772
C_9	-4.387818
C_{10}	2.463391
C_{11}	1.161813
C_{12}	0.396901
C_{13}	3.111346
C_{14}	0.805387

crust and 1.73 in the uppermost mantle (Mukhopadhyay et al. 1997; Bhattacharya et al. 2005; Baruah et al. 2010). Depth to the Conrad is fixed at 19 km (Baruah et al. 2010). The velocity model used in this study is schematically shown in Fig.7.

5 RESULTS

5.1 Reflected phases

As illustrated above the reflected phases (PmP-P and SmS-S) are used in the inversion program. Acceptable results are obtained after five iterations. The root mean square (RMS) of residuals for the initial model was 0.353 s and it reduced to 0.308 s after five iterations.

Table 3 Inverted values of unknown parameters for the Moho depth using reflected and converted phases

Coefficients	Values
C_0	39.155318
C_1	-5.831189
C_2	4.680860
C_3	-3.918051
C_4	-6.289086
C_5	-3.985771
C_6	5.218436
C_7	-1.661528
C_8	3.928286
C_9	-6.896948
C_{10}	2.781078
C_{11}	1.777965
C_{12}	0.727927
C_{13}	2.40824
C_{14}	4.088746

Estimated values of the coefficients C_K are listed in Table 2. The Fig. 8 shows the Moho depth at each reflection point and the Fig. 9 shows the spatial distribution of reflection points indicating the travel time residuals between observed and theoretical travel times. The contour plot of Moho depth is shown in Fig. 10**;** the Moho depth varies from 33.5 to 41.5 km beneath the study area.

5.2 Reflected and Converted Phases

Estimation of Moho depth is improved using both the converted phases and reflected phases**.** The solution converged in five iterations, and the RMS values reduced from 0.351 s to 0.287 s. This result shows that the depth of the Moho is deeper beneath the Brahmaputra valley and shallower beneath the Shillong plateau (Fig. 11). Depth distribution of Moho is illustrated in Fig 12; it shows that the Moho depth varies from 33 to 41 km in the study region. The estimated values of co-efficient C_K are listed in Table 3. The Fig. 13 shows the spatial distribution of reflection and conversion points that are relatively uniformly distributed in the study area.

6 Discussion

The Moho depth is estimated in Shillong-Mikir Hills region in northeast India using travel time differences between reflected P (PmP), S (SmS) and converted P to S (PS), S to P (SP) waves. We have used the inversion model of Nakajima et al. (2002) with the consideration of epicentral distance ranging from 70 km to 200 km. The reflection and the conversion points are fairly well distributed in the study area. The prominent features in Moho configuration illustrate thinner crust (~33 km) in the western part of the Shillong plateau in the Garo Hills region, which was the rupture area of the 1897 great Shillong earthquake. The thinner crust may be the result of pop-up tectonics of the plateau (Bilham and England, 2001). The Moho depth beneath Brahmaputra valley is 5-8 km deeper than that in the Shillong area. This observation is comparable with the earlier studies by receiver function analysis (Kumar et al. 2004; Mitra et al. 2005). Sitaram et al. (2001), estimated the Moho depth at (45.3±1.4) km using the Pg, P* and Pn waves.

Similar observations were also reported by Gaur and Bhattacharya (1983) and Verma and Mukhopadhyay (1977) from the Bouguer gravity anomalies. The deeper Moho depth beneath the Brahmaputra valley indicates under thrusting of the Indian plate below Himalaya. Kumar et al. (2004) and Mitra et al. (2005) reported the Moho depth below the Shillong Plateau at 35-38 km and that below the Brahmaputra valley is deeper by ~ 5-7 km. Bora and Baruah (2012) estimated the Moho depth (35-38) km beneath the Shillong plateau. Nayak et al. (2008) by gravity modeling suggested that the Moho beneath the Shillong plateau is at ~ 35 km compared to that ~ 42 km below the Bengal basin to the south and Assam valley to the north. All these earlier estimations are fairly consistent with the present study as summarized in Table 4, except the higher crustal thickness estimated by gravity modeling by Verma and Mukhopadhyay (1977) and Rajasekhar and Mishra (2008). The seismic activity indicates that the lower crust beneath the Shillong and Mikir plateau is intensively active. Upper most mantle seismic activity down to 50 km is also

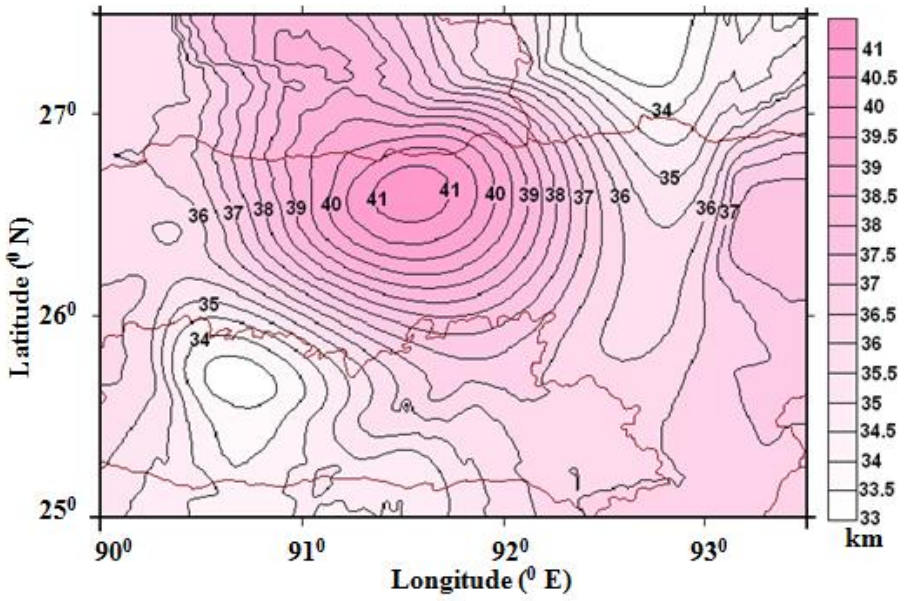

Figure 12. Depth distribution of Moho obtained at the reflection and conversion points. Depth to the Moho is shown by contours with 0.5 km interval. The corresponding color scale is shown along with.

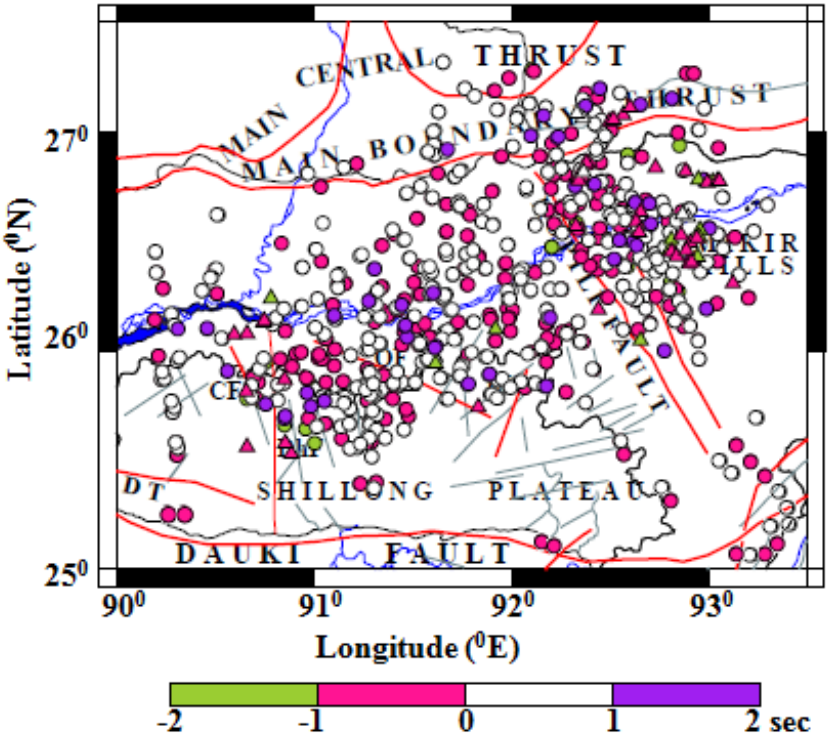

Figure 13. Distribution of reflection and conversion points at the Moho. Circles and triangles denote reflection and conversion points, respectively. Color scale at each point shows travel time residual between observed and theoretical travel time difference.

reported by local microearthquake network data (Kayal 2001) and also by teleseismic network data (Chen and Molnar, 1990). The clear P-S and S-P converted phases are well

Table 4. A list comprising the depth of Moho in Shillong and Mikir Hills Plateau, NER, India

Tectonic Blocks	Depth of Moho (Km)	Methodology	Reference	Year
Shillong Plateau	35±1	Receiver Function Analysis	Kumar et al.,	2004
	35	Receiver Function Analysis	Mitra et al.,	2005
	35±2	Gravity Modeling	Nayak et al.,	2008
	37-38	Gravity Modeling	Rajasekhar & Mishra	2008
	30±1	Travel-time analysis	Baruah et al.	2010
	(35-37) ±0.5	Inversion of Travel Time Residuals	**Present Study**	
Mikir Hills	34±4(DMK)	Receiver Function Analysis	Kumar et al.,	2004
	35±1	Travel-time analysis	Baruah et al.	2010
	(37.5-38.5) ±1.0	Inversion of Travel Time Residuals	**Present Study**	
Assam Valley	35±3(JPA) 35±3(TZR)	Receiver Function Analysis	Kumar et al.,	2004
	42 (TZR) 40 (GAU)	Receiver Function Analysis	Mitra et al.,	2005
	42(Assam valley to the North)	Gravity Modeling	Nayak et al.,	2008
	(35-37) ±1.0 (36-38) ±0.5 (39-41) ±0.5	Inversion of Travel Time Residuals	**Present Study**	

identified from the deeper depth earthquakes in this study, and these data provided useful information in our study.

7 Conclusion

We estimated the Moho depth distribution beneath the Shillong – Mikir plateau using travel time data of reflected and converted waves at the Moho. The reflected P- and S- waves at the Moho are observed in three component seismograms from shallow (depth $\leq$ 25 km) crustal earthquakes. The P- to –S and S- to –P converted waves at the Moho are also observed from deeper (depth < 38 km) earthquakes. The Moho depth is estimated by using travel time differences between these later phases and the first P- and S- wave arrivals.

The estimated Moho depth in the central part of Shillong plateau are shallower (33-35 km) while most part of the Mikir hills and Brahmaputra valley indicate deeper (39-41 km) Moho.

Acknowledgements

Data obtained from NEIST, Jorhat; NGRI, Hyderabad; IIG, Mumbai and Gauhati University are acknowledged. We appreciate the kind help by Junichi Nakajima, Associate Professor, Tohoku University, Sendai, Japan for providing his code and valuable suggestions during this study. Sincere thanks to Prof. J. R. Kayal, Emeritus Scientist, Jadavpur University, Kolkota, India for his valuable suggestions during this work. We also thank the anonymous reviewers for their useful comments.

References

Angelier, J., and S.Baruah (2009). Seismotectonics in Northeast India: a stress analysis of focal mechanism solutions of earthquakes and its kinematic implications, *Geophysical Journal International,* 178, 303-326.

Baruah, S., R. Duarah, and D.K.Yadav (1997). Pattern of seismicity in Shillong Mikir plateau and the orientation of compressional axis, *Journal of Geological Society of India,* 49, 533-538.

Baruah, S. , and D.Hazarika (2008). A GIS based Tectonic Map of India, *Current Science*, 95,176-177.

Baruah, S., D.K. Bora, and R.Biswas (2010). Estimation of crustal discontinuities from reflected seismic waves recorded at Shillong and Mikir Hills Plateau: Northeast India, *International Journal of Earth Sciences*, doi:10.1007/s00531-010-0541-2.

Bhattacharya, P. M., J. Pujol, R. K. Mazumdar, and J.R. Kayal (2005). Relocation of earthquakes in the Northeast India region using joint Hypocenter determination method, *Current Science,* 89 (8), 1404-1413.

Bhattacharya, P. M., S. Mukhopadhyay, R.K. Mazumdar, and J.R.Kayal (2008). 3-D seismic structure of the northeast India region and its implication for local and regional tectonics, *Journal of Asian Earth Sciences,* 33, 25-41.

Bhattacharya, P.M., J.R.Kayal, S. Baruah, and S. S. Arefiev (2010). Earthquake source zones in northeast India: seismic tomography, Fractal dimension and b value mapping, *Pure and Applied Geophysics,* doi: 10.1007/s00024-010-0084-2

Bilham, R. , and P. England (2001). Plateau "pop-up" in the Great 1897 Assam earthquake, *Nature,* 410, 806-809.

BMTPC (2003) Vulnerability atlas- 2nd edn; peer group MoH & UPA; seismic zones of India IS: 1983-2002, BIS, GOI, Seismotectonic atlas of India and its environs, GSI, GOI.

Bora, D.K., S. Baruah (2012). Mapping the crustal thickness in Shillong-Mikir Hills Plateau and its adjoining region of northeastern India using Moho reflected waves, *Journal of Asian Earth Sciences,* 48, 83-92.

Chen, W.P., and P. Molnar (1990). Source parameters of earthquakes and intraplate deformation beneath the Shillong Plateau and northern Indo Burma ranges, *Journal of Geophysical Research,* 95,12,527-12,552.

Dasgupta, A., and A.K. Biswas (2000). Geology of Assam, *Geological Society. of India*, pp. 170, Bangalore, India.

De, R, and J.R. Kayal (1990). Crustal P-wave velocity and velocity-ratio study in Northeast India by a microearthquake survey, *Pure and Applied Geophysics,* 134, 93-108.

Evans, P. (1964). Tectonic framework of Assam, *The Journal of the* Geological Society *of* India, 5, 80- 96.

Gaur, V.K., and J. C. Bhattacharya (1983). Gravimetric determination of the shape of Mohorovicic discontinuity in Peninsular and north-eastern India. Paper presented at I.U.G.G. General Assembly at Hamburg, Germany, Aug. 15-27.

Horiuchi, S., H. Ishii, and A. Takagi (1982a). Two-dimensional depth structure of the crust beneath the Tohoku district, the northeastern Japan arc. I. Method and Conrad discontinuity, *Journal of physics of Earth.* 30, 47–69.

Horiuchi, S., A. Yamamoto, A. Ueki, K. Tachibana, T. Kono, and A. Takagi (1982b). Two dimensional depth structure of the crust beneath the Tohoku district, the northeastern Japan arc.II. Moho discontinuity and P-wave velocity, *Journal of Physics of Earth,* 30, 71-86.

Kayal, J.R., and R. De (1991). Microseismicity and tectonic in Northeast India, *Bulletin of the Seismological Society of America,* 81,131-138.

Kayal, J.R. (1996). Earthquake source process in northeast India: A review, *Journal of Himalayan Geology,* 17, 53-69.

Kayal, J.R., and D. Zhao (1998). Three dimensional seismic structure beneath Shillong Plateau and Assam Valley, northeast India, *Bulletin of the Seismological Society of America,* 88, 667-676.

Kayal, J.R. (2001). Microearthquake activity in some parts of the Himalaya and the tectonic model, *Tectonophysics*, 339, 331-351.

Kayal, J.R., S.S. Arefiev, S. Baruah, D. Hazarika, N. Gogoi, A. Kumar,S.N. Chowdhury and S. Kalita (2006). Shillong Plateau Earthquakes in Northeast India region: Complex tectonic model, *Current Science.* 91, 109-114.

Kayal, J.R. (2008). Microearthquake Seismology and Seismotectonics of South Asia, *Springer,* pp 273-275.

Kumar, M.R., P.S. Raju, E.U. Devi, J. Saul, and D.S. Ramesh (2004). Crustal structure variations in northeast India from converted phases, *Geophysical Research Letters,* 31, 1-4, doi: 10.1029/2004GL020576.

Lienert, B.R., B.E.Berg, and L. N. Frazer (1986). Hypocenter: An earthquake location method using corrected, scaled and adaptively damped least squares, *Bulletin of Seismological Society of America* ,76,771-783.

Matsuzawa, T., N. Umino, A. Hasegawa, and A. Takagi (1986). Upper mantle velocity structure estimated from PS-converted wave beneath the northeastern Japan arc, *Geophysical Journal of Royal. Astronomical Society,* 86, 767–787.

Matsuzawa, T., T. Kono, A. Hasegawa, and A. Takagi (1990). Subducting plate boundary beneath the northeastern Japan arc estimated from SP converted waves, *Tectonophysics*, 181, 123–133.

Mitra, S., K. Pristley, A. Bhattacharya, and V. K. Gaur (2005). Crustal structure and earthquake focal depths beneath northeastern India and southern Tibet, *Geophysical Journal International,* 160, 227-248.

Mukhopadhyay, S., R. Chander, and K. N. Khattri (1997). Crustal properties in the epicentral tract of the Great 1897 Assam Earthquake, northeastern India, *Tectonophysics,* 283, 311-330.

Nakajima, J., T. Matsuzawa, A. Hasegawa (2002). Moho depth variation in the central part of northeastern Japan estimated from reflected and converted waves, *Physics of Earth and Planetary Interiors,* 130, 31-47.

Nandy, D.R. (2001). Geodynamics of Northeastern India and the adjoining region, *ACB publication, Calcutta*, pp 209.

Nayak, G.K., V. K. Rao, H. V. Rambabu, and J. R. Kayal (2008). Pop-up tectonics of the Shillong Plateau in the great 1897 earthquake (Ms 8.7): Insights from the gravity in conjunction with the recent seismological results, *Tectonics*, 27, 1-8, doi: 10.1029/2006TC002027.

Okada, H., S. Suzuki, and S. Asano (1970). Anomalous understanding structure in the Matsushiro earthquake swarm area as derived from a fan shooting technique, *Bulletin of Earthquake Research Institute*, 48, 811-833.

Oldham, R.D. (1899). Report on the great earthquake of the 12th June 1897, *Memoirs of Geological Survey of India,* 29, 1-379.

Ohmi, S. and S. Hori (2000). Seismic wave conversion near the upper boundary of the Pacific plate beneath the Kanto district: Japan, Geophysical *Journal International,* 141, 136-148.

Rai, S.S., K. S. Prakasam, and N. Agarwal (1999). Pn wave velocity and Moho geometry in north eastern India, *Journal of Earth System Science,* 108, 297-304.

Rajendran, C.P., K. Rajendran, B. P. Duarah, S. Baruah, and Anil Earnest (2004). Interpreting the style of faulting and paleoseismicity associated with the 1897 Shillong, northeast

India:Earthquake: Implications for regional tectonism, *Tectonics,* 23, 1-12, doi: 10.1029/2003TC001605.

Rajasekhar, R.P. , and D. C. Mishra(2008). Crustal structure of Bengal Basin and Shillong plateau: Extension of Eastern Ghat and Satpura Mobile Belts to Himalayan fronts and seismotectonics, *Gondwana Research*, 14, 523- 534.

Ramesh, D.S., M. R. Kumar, E. U. Devi, P. S. Raju, and X. Yuan(2005). Moho geometry and upper mantle images of northeast India, *Geophysical Research Letters,* 32, 14301-14304.

Sitaram, M.V.D., G. John, P. G. Rao, and M. M. Saikia(1986). Pn wave velocities in the uppermost mantle beneath northeast India.In:S.K.Guha (Ed.), Earthquake Prediction-Present status. University of Poona, India, pp. 267-275.

Sitaram, M.V.D., D. K. Yadav, and K. Goswami(2001). Study on crustal structure beneath Arunachal Himalaya and Assam, *Journal of Geological Society of India,* 58, 285-301.

Tapponnier, P., G. Peltzer, A.Y. Le Dain, R. Armijo, and P. Cobbold(1982). Propagating extrusion tectonics in Asia: New insights from simple experiments with plasticine. Geology, 10,611-616.

Tillottson, E. (1953). The great Assam earthquake of 1950, the completion of papers on the Assam Earthquake of August 15, 1950, Compiled by M.B.Ramachandra Rao, pp 94-96.

Verma, R.K. , and M. Mukhopadhyay(1977). An analysis of the gravity field in northeastern India, *Tectonophysics*, 42, 283-317.